Environmental Research & Technology
https://ertjournal.org/index.php
DOI: https://doi.org/10.35208/ert.1685945

ECHO ACADEMIC PUBLISHING
The Echo of Scientific Knowledge

RESEARCH ARTICLE

AI techniques for feature extraction, simplification and aggregation geospatial data

Polina LEMENKOVA [1, 2, 3, 4, *]

[1] *Bureau de Recherches Géologiques et Minières (BRGM), 3 Avenue Claude-Guillemin, 45060 Orléans, France*

[2] *Le Studium, Institut d'Études Avancées du Val de Loire, 1 rue Dupanloup, 45000 Orléans, France*

[3] *Le laboratoire PRISME, Institut National des Sciences Appliquées de Centre-Val de Loire (INSA CVL, UR 4229), Université d'Orléans, Château de la Source, 45100 Orléans, France*

[4] *La Technopole d'Orléans, 1 Avenue du Champ de Mars, 45100 Orléans, France*

ARTICLE INFO

Article history
Received: 28 April 2025
Revised: 29 September 2025
Accepted: 30 September 2025

Key words:
Remote sensing, artificial intelligence, machine learning, random forest, cartography

ABSTRACT

This study proposes an Artificial Intelligence (AI) application to cartographic workflow with the purpose of environmental mapping. The Random Forest (RF) framework of Machine Learning (ML) was applied to satellite image analysis for detection and robust attribution of biodiversity changes in Africa. Changes in land cover types were investigated on Landsat using comparison of several algorithms integrated in data processing and cartographic scripts using Geographic Resources Analysis Support System (GRASS) Geographic Information System (GIS). The analysis of time series highlights biodiversity changes in north Namibian landscapes in relation to presumed impacts of multiple potential environmental drivers: climate-related factors in desert setting (high fluctuations in temperature, salt crust in the saline lake and low precipitation) and anthropogenic forces (land use, abandoned areas and agriculture). The computational results demonstrated following outcomes. According to the calculated number of pixels corresponding to the cells in the raster images covering the Etosha landscapes, the land use types demonstrated the following changes: 1. Mosaic vegetation and cropland (8.42%), Aquatic or regularly flooded vegetation decreased on 13,59% due to seasonal fluctuations, areas of artificial surfaces declined insignificantly (2.40%), Mixed broadleaved deciduous forests experienced slight decreasd (1.18%), and the class of open grasslands increased to 5.32 %. Moreover, rainfed croplands demonstrated stable development with 4.58% of changes, while salt hardpans changed significantly to 12, 73%. Finally, water bodies including Etosha basin decreased significantly due to the seasonal effects (21.73%), Herbaceous vegetation, shrubland and thickets developed relatively stable with minor changes not exceeding 3.25 %, and sparse savannah grasslands occupied similar areas with fluctuations not exceeding 4,72%. The accuracy of image classification was evaluated by kappa statistics and chi-square against the ground truth data obtained from the land cover and soil data inventory. The original data with Land Use Land Cover (LULC) thematic classes were reclassified into 10 categories. The results show variations in land cover change due to arid desert climate in northern Namibia. This provides evidence of biodiversity changes in Africa detected using AI-driven data analysis using multispectral satellite images.

Cite this article as: Lemenkova P. AI techniques for feature extraction, simplification and aggregation geospatial data. Environmental Research and Technology, 2026, 9 (4), 677-692.

INTRODUCTION

Identifying changes in land cover types is a critical issue for sustainable land management in protected areas [1-4]. Understanding landscape dynamics using remote sensing (RS) data is a challenge since it involves the complexity of factors that affect the shape of the Earth. Satellite image analysis is effective tool for landscape mapping since it assists environmental planning and decision making for sustainable development. Image analysis involves complex tasks of extracting information from the satellite data. The state-of-the-art (SOTA) methods of RS data processing are based on cartographic Geographic Information System (GIS) tools to extract, process and interpret geo-information [5-6]. To facilitate complex data processing workflow, machine learning (ML) algorithms support RS data processing through improved accuracy and speed of data processing, and level of automation and precision [7-9].

Current literature on geoinformatics reports existing cases of the successful application of GeoAI to image analysis. Among

* Corresponding Author: polina.lemenkova@tech-orleans.fr (Polina Lemenkova)

others, the following approaches are tested and employed: Pyramid scene parsing network (PSPNet) [10], DeepLabV3 (PyTorch) [11-12], UNet [13-15], TensorFlow and Keras [16-17], Segment Anything Model (SAM) Meta-AI [18], algorithms embedded in Python's Scikit-Learn library [19-21], TensorBoard open source toolkit in ArcGIS (API for Python). Such technical methods enable to do semantic segmentation modelling of the images and feature extraction on the scenes for pattern recognition in the environmentally constraint regions [22-24].

This paper presents the use of Artificial Intelligence (AI) as an advanced approach to the RS-based environmental mapping. Specifically, we present the case of monitoring land cover changes in protected ecosystems of northern Namibia. Land cover changes were visualised and evaluated using time series of satellite images in one calendar year (2022) processed by ML methods. This study presents an interdisciplinary, data-driven project aiming at understanding the environmental trends of plant biodiversity in northern area of Namibia. The selected area is located around saline lake Etosha and undergoes a spontaneous process of increased arid climate, desertification and salinization [25-28].

This study focuses on monitoring landscapes of the Etosha lake surroundings using ML for RS data processing. The analysis of the time series of Landsat scenes taken in 2022 illustrated the process of water evaporation and its gradual replacement by salt and minerals during a calendar cycle from wet to dry periods in Namibia. Using RS data processed by AI/ML methods in Geographic Resources Analysis Support System (GRASS) GIS, we seek to assess the feasibility of measuring fluctuations in salt/water level and associated land cover changes around the Etosha lake, Namibia.

STUDY AREA

Three protected areas span northern Namibia: 1) Etosha National Park (including saline lakes Etosha Pan and Natukanaoka Pan); 2) Waterberg Plateau National Park; 3) Landscapes of Shana region including Reserve nature areas: Onguma and Ongava, Namibia. Etosha Lake is the saline protected lake located in north Namibia, Figure 1. It has a unique hydrological and ecological setting [29-30].

In the dry periods, the areas of lake can be covered by salt crust, while in the wet periods, this ephemeral lake presents the precious source of water for migrating birds, e.g., flamingoes [31] and rare species [32-33]. The mean annual rainfall ranges from 250 mm/year in the west and up to 550 mm/year in the east [34]. The lake is generally shallow. The eastern part of the Etosha lake basin is wet and deeper in terms of topographic setting. Such differences in the structure of the basin affect local climate setting.

Variations in landscapes around Etosha are affected by the composition and distribution of plant biodiversity [35-36]. Understanding changes in land cover types enables to highlight areas of maximum compositional change and to quantify the percentage of rare African species for which landscape restoration has substantially improved or worsened conservation prospects [37-38]. The salinization of the saline lakes is relatively high in the periods of droughts that cause dissolution of salts through water evaporation which increases the Potential of Hydrogen (pH) [39-42]. In contrast, during the occasional rains, the convective clouds appearing over the lake with peaks in the winder period cause thermal inversions, which lead to higher occurrence of precipitation in the coastal areas influenced by seasonal climate patterns, mostly during winter.

For arid climate of Namibian, scarce resources of groundwater that are maintained by the Etosha lake, help vegetation and savannah grasses to keep a certain amount of water in the leaf area, and to grow during periods of drought. These two features led to a large capacity of the vegetation canopy, particularly in the savannah fields and scarce forests, to intercept liquid precipitation, release only a small amount of precipitation to the soil and eventually to maintain runoff in groundwater. These processes contribute to the sustaining of different types of soil, Figure 2. Land cover types change as a function of geographical distances, ecological dissimilarities, and differences in climate setting. Landscapes of the Etosha National Park are dominated by the distribution of dry savannah which is a typical environmental characteristics of Namibia [43-44]. Etosha National Park has high evapotranspiration level typical for arid climate and associated reduction of the sensible heat flux during the periods of droughts in north Namibia. However, accurate estimation of the amount of water which was intercepted by the Salt Lake Etosha Pan and subsoil remains a direction for further research and requires direct hydrogeological observations with relevant equipment.

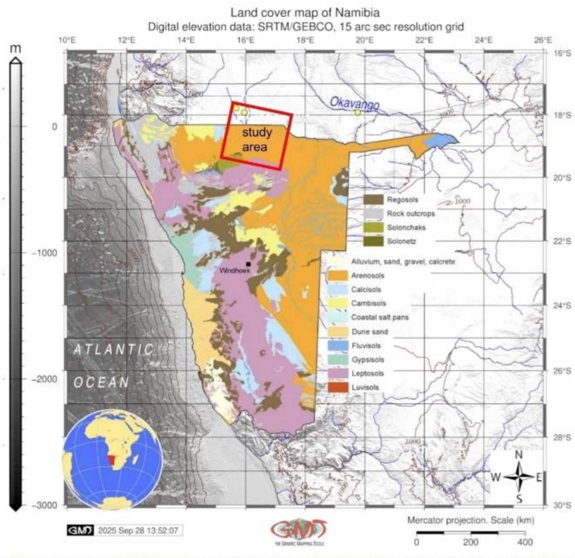

Figure 1. Environmental map of soil types in Namibia and the study area (rotated red square) indicating the location of the satellite images Landsat 8-9 OLI/TIRS

METHODS

In this study, we employed the AI/ML methods of geospatial data processing for generalizing and measuring pixel-wise land cover changes as numerical output (computed percentage) and as cartographic visualization (maps). The technical workflow included tasks of scene classification, object detection on the satellite images, image segmentation and information extraction. Specifically, we employed the advancements of GRASS GIS software to facilitate monitoring of landscape dynamics in Namibia. This project builds a Python-based ML modelling to employ novel algorithms of pattern recognition across the time series of satellite images. The use of the supervised classification eliminates these errors by precisely assigning pixels to different classes, as noted earlier [45-47]. After calibrating the AI-driven models with collected RS data, we created maps of landscape dynamics over Etosha at different times. The comparison of the maps allowed highlighting the areas where changes in land cover induced the largest changes in wildlife species composition, and quantifying the consequences for regional plant diversity in Namibia.

Objectives and Goals

This study focuses on environmental monitoring of Namibia, southern Africa. The study has three major scientific objectives. First of all, to assess how temporal changes in land cover types over Etosha varied over time during one calendar year (2022). Second, to apply the AI/ML-driven algorithms for image analysis processing to identify multiple ecological pressures that caused changes in habitats and biodiversity. Third, to process cartographic data and classifying time series image analysis for dissimilarity modelling aimed at modelling salt/plant assemblages over Etosha Lake. To achieve these goals, the technical objective is to improve the accuracy, increase the speed and reduce the complexity of the workflow in RS data processing with the case of environmental mapping of southern region of Africa. To this end, we employ the ML algorithms of computer vision for pattern recognition and image analysis.

The motivation of this study is to reveal environmental changes in vegetation in the landscapes in Namibia during recent decades that experienced the effects of climate change. Specifically, these included land cover changes, decline of vegetation and ecosystem degradation in the drought-prone areas of the saline Etosha lake. By analysing six multispectral satellite images, we quantified variations in land cover types in target period that refer to the biodiversity gradients in Namibia. With this regards, the project has been designed, and is conducted to reinforce the environmental goals, that include the following issues.

Data

The data were collected from the EarthExplorer repository, United States Geological Survey (USGS) and include 8 satellite images Landsat Operational Land Imager/Thermal Infrared Sensor (OLI/TIRS). The scenes were collected from March to August in 2022. The images have 185*185 km geographical extent for each Landsat 8-9 OLI/TIRS scene, 30 m spatial resolution for multispectral bands and minimal cloudiness (below 10%).

The dataset includes satellite data (Landsat imagery) covering various periods for time series analysis. The original images are visualized in Figure 2.

To process the data, we employ advanced methods of Geospatial Artificial Intelligence (GeoAI). A series of satellite images was used to estimate the areas of changes in the lake basin according to the annual land cover changes and ecosystem components based on data measured in 2022 using RS data at the Landsat data were processed into Collection 1. Major technical characteristics that differ for each Landsat scene are provided in Table 1. The data were obtained from the EarthExplorer repository of the United States Geological Survey (USGS) as reliable data source used in previous studies [48-50]. The dataset included six satellite images of the Landsat 8-9 Operational Land Imager and Thermal Infrared Sensor (Landsat 8-9 OLI/TIRS) with 30-m resolution. The images were taken during the day period with nadir on at Worldwide Reference System (WRS) Path 179, WRS Row – 73 of the Landsat satellite sensors.

Software

Three Geographic Information System (GIS) software were used in this study: Quantum GIS (QGIS), Generic Mapping Tools (GMT) scripting toolset and GRASS GIS. The application of this software in cartographic domains is widely used [51-54] which proves robust methods for RS and spatial data analysis. The QGIS software was used for land cover mapping to represent the geospatial information of the landscape. The GMT was used to map topographic information and visualise the location of the study area in northern Namibia using overlaid extent of the multispectral Landsat images. Colour composites were generated in GRASS GIS using 'r.composite' module and visualised in Figure 3.

Metadata include major technical characteristics of the satellite images which common for all the scenes are as follows: Landsat Collection Category – T1, Collection Number 2, Data Type L2 – OLI_TIRS_L2SP; Sensor Identifier – OLI/TIRS; Station Identifier – LGN. Product Map Projection L1 for all the scenes is Universal Transverse Mercator (UTM) Zone 33 for northern Namibia, with Datum and Ellipsoid – WGS 84 (World Geodetic System 1984) . The Ground Control Points (GCP) Version for all the images is 5. The images were preprocessed by the provider using Landsat Product Generation System (LPGS) Processing Software Version 15.6.0 for Landsat-8 scenes and 16.2.0 for Landsat-9 scenes, respectively. Technically, the LPGS generates the data products of Landsat in GeoTIFF output format using standard image parameters. Cubic Convolution (CC) resampling method was applied to all images in most of the spectral bands and a spatial coverage of 185 km swath for each Landsat scene. The digital numbers (DN) were converted to surface reflectance. To this end, the DNs were first converted to radiance using sensor-specific metadata. Afterwards, top-of-atmosphere (TOA) reflectance was converted using the information on sun-sensor geometry and solar irradiance recorded in the metadata of the satellite images.

The procedures were performed using 'i.landsat.toar' modul which reads the values of cells as discrete, bit-encoded representations of the original analog data. Using the 'i.landsat.toar' module, the pixels were converted into physical units of spectral reflectance through calibration factors that were used laters on for quantitative raster analysis. The GMT was used using scripting techniques. The extent of the images is denoted by the rotated square showing the location of the Landsat scenes. Their coordinates were derived from the metadata and correspond to the technical parameters of the Landsat mission. The Geographic Resources Analysis Support System (GRASS) GIS software was used for RS data processed by AI/ML methods of diverse modules using scripting techniques.

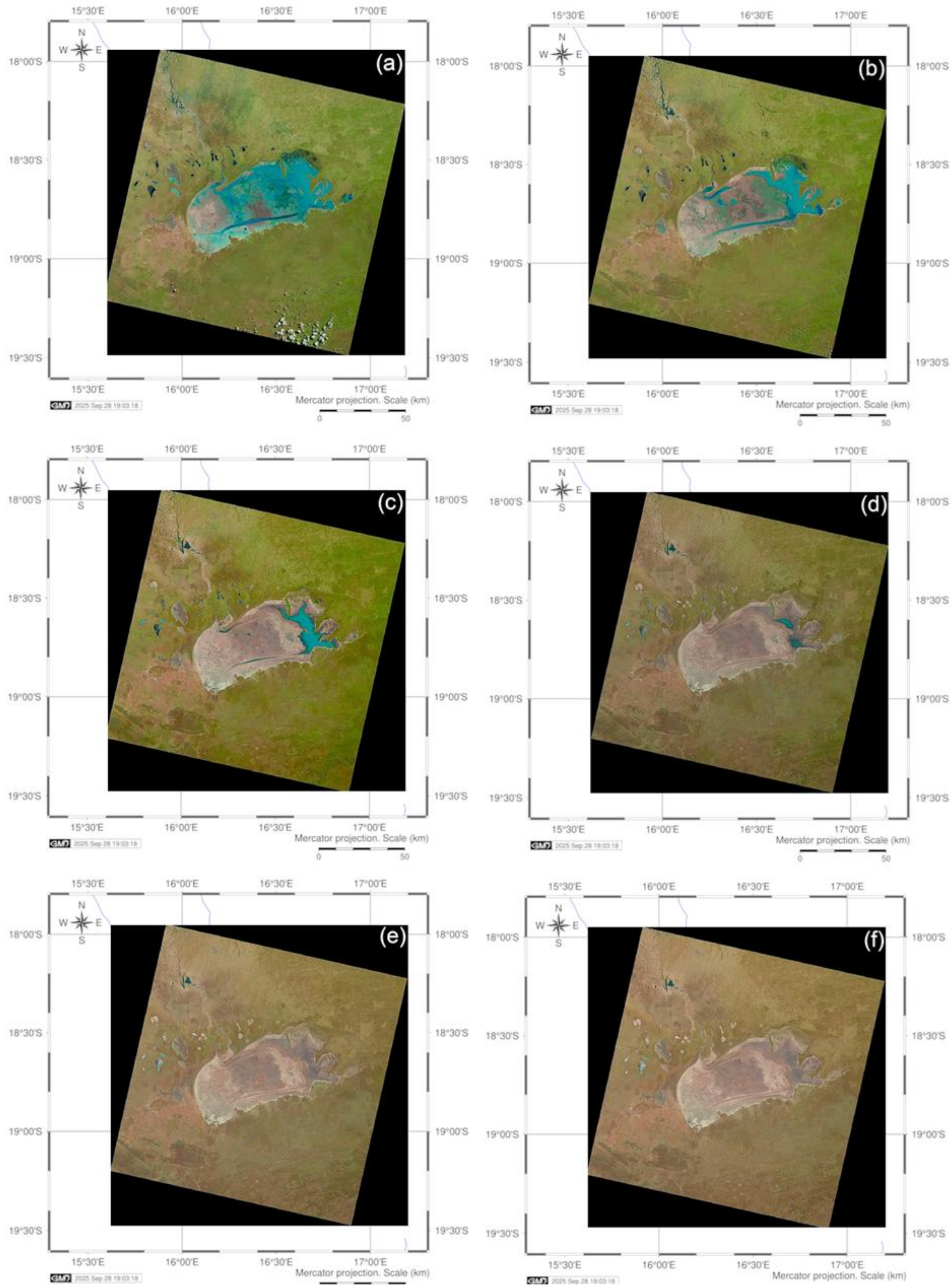

Figure 2. Drying Etosha lake: seasonal fluctuations of water level from wet period (spring) to extreme heat (late summer). Original RS data: multispectral satellite images Landsat 8-9 OLI/TIRS. Data source: United States Geological Survey (USGS)

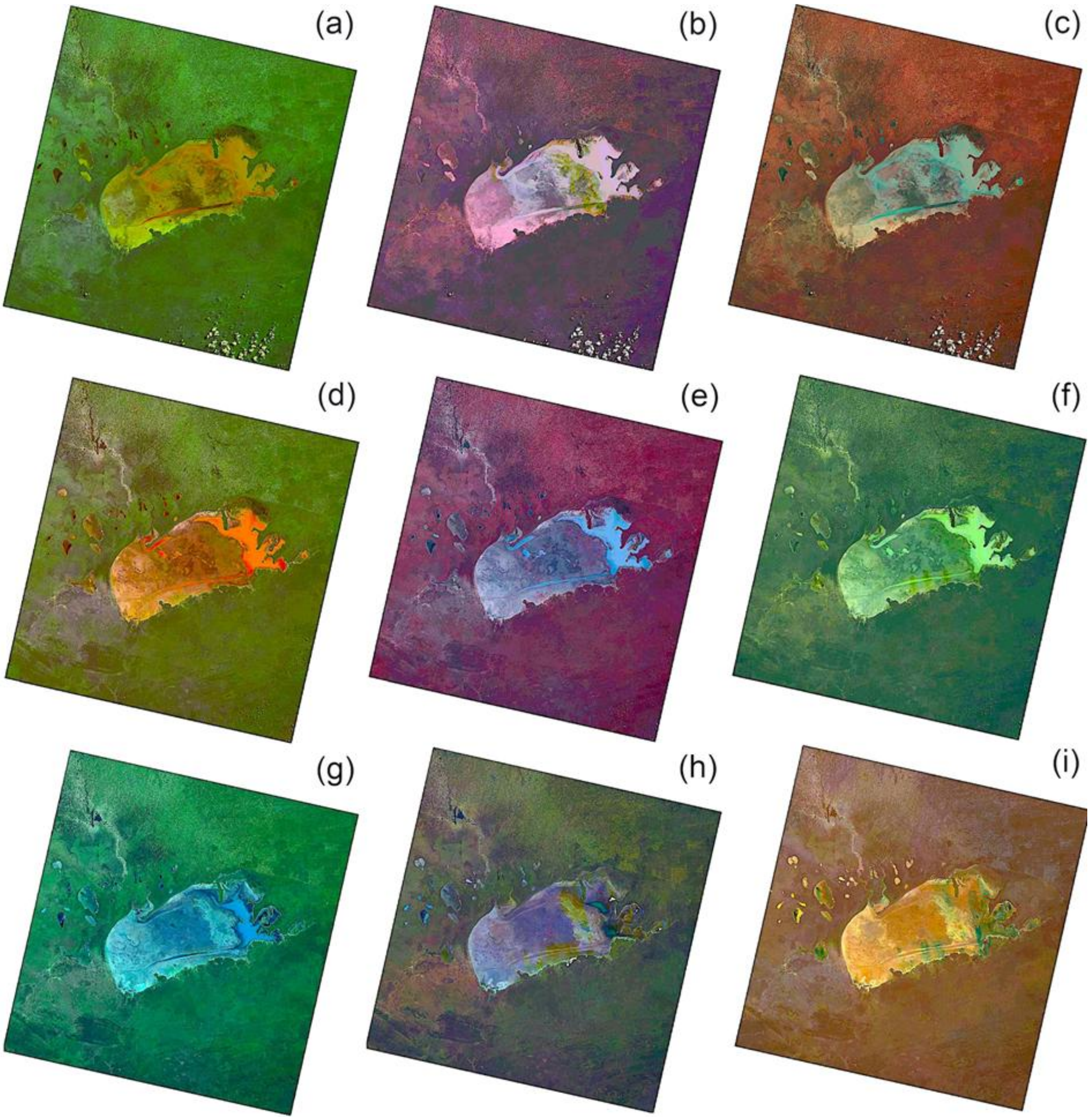

Figure 3. Colour composites of multispectral bands of the satellite images Landsat 8-9 OLI/TIRS (2022)

Workflow

Image processing

The class distribution of pixels in the original multispectral colour images were computed and summarized by module of GRASS GIS in the statistical report for each image. Colour composites were generated for classification approach based on information on pixel reflectance derived automatically using computer vision algorithms during the classification processes for maximum likelihood and random forest (RF) algorithms [55]. Green colours indicate mosaic vegetation in the surrounding landscapes, Figure 3.

The workflow identifies five algorithm steps of image processing and classification — 1) Support Vector Machine (SVM), 2) Multi-layer Perceptron (MLP) Classifier of the Artificial Neural Network (ANN), 3) Decision Tree Classifier (DTC), and 4) Random Forest (RF). After evaluation following the existing methods [56], we selected RF as the best method. Other statistical values included estimated minimum class size and class separation for each image and sampling interval in order to quantitatively evaluate how correct the pixels were assigned into the given land cover categories. This was performed using the evaluation of class separability presented in matrices showing difference between 10 classes for spring and autumn 2019, 2022 and 2023, respectively. Here classes correspond to the following categories: 1) Mosaic vegetation / cropland 2) Aquatic or regularly flooded vegetation; 3) Bare areas and artificial surfaces; 4) Mixed broadleaved deciduous forests; 5) Open grassland; 6) Rainfed cropland; 7) Salt hardpans; 8) Water bodies (Etosha basin and lakes); 9) Herbaceous vegetation, shrubland and thickets; 10) Sparse savannah grasslands.

Different colour composite combinations highlighting the Etosha Pan, Namibia are shown in Figure 4. These images are generated based on triplets of Landsat 8-9 OLI/TIRS bands by 'r.composite' module of GRASS GIS: (a): March: Bands 7-5-3; (b): March: Bands 2-3-4; (c): March: Bands 3-4-5; (d): April: Bands 7-5-4; (e): April: Bands 3-4-5; (f): April: Bands 3-4-5;

(g): May: Bands 3-5-7; (h): June: Bands 1-5-6; (i): August: Bands 7-4-1.

The standard deviations and means for seven bands of image regions were employed to evaluate the weights of the spectral reflectance of pixels and texture features represented on the images. The initial means for each band of the textured mosaic images were computed for each image composed of the classified images of the texture composites, Figure 6. The estimation of positive correctness is performed according to the module embedded in GRASS GIS. Specifically, the script used RF model using r.learn.train module for RF algorithm of image processing.

Context information

We used the class separability matrix for extraction of pixels according to the computed feature classes using several iterations. The number of stable points were computed for each image, and the convergence represented more than 98% for each scene. In general, the automatic tracing of pixels by ML. libraries of GRASS GIS performed well for the segments of landscape patches that belong to different land cover classes. For the cases where the DNs of pixels overlap due to the similar spectral reflectance, large zooming of the maps was added to correct the misclassified pixels. Here we corrected the classification using zooming, followed by time reclassification, and cross-validation. The accuracy analysis shows the rejection probability for classified pixels. Specifically, it shows the uncertainties in the automated pixel grouping through visualized precision maps.

AI-based modeling

In the process of RF refinement, the following procedures were completed using supervised learning model 'RandomForestClassifier'. First, training areas were created from the 'trainingmap' where the results of the clustering raster map with labelled pixels assigned to 10 classes were used as balanced training data using class weights. Such adjustment enabled to automatically refine weights inversely proportional to class frequencies of pixels in each raster of the classified Landsat image. Second, the standardized feature variables were converted into values of zero mean and unit variance to reduce the complexity of computations. The classification results show that spectral distributions of the pixels discriminated some regions within the Etosha Pan more precisely compared to the MaxLike and clustering approaches. The class probabilities were predicted using the 'r.learn.predict' module. Third, feature importances were computed using permutation of pixels which were placed in a discrete raster around the boundary study area to increase the accuracy of computation. The classified land cover patches were highlighted by random colour palette and corresponded to the different land cover types in the image covering Etosha surroundings.

Accuracy assessment

For RS, accuracy assessment and validation include the estimation of correctness of image classification. In this case, it was computed using splitting the raster dataset into the group categories of pixels where each pixel is defined to be suitable to the specific cluster according to its spectral reflectance value. The accuracy assessment was performed using computed Kappa statistical based on the evaluated DNs. The goal of accuracy assessment is to quantitatively evaluate the proportion of pixels correctly assigned to a given land cover category. The assessment included the output maps made with the six satellite scenes and validated the results using following approaches: 1) Overall accuracy of the maps generated using satellite images covering Etosha; 2) User's accuracy of each of the classes; 3) Kappa coefficient for identification of misclassified pixels.

The class means Digital Numbers (DN) of pixels computed for pixels assigned to 10 land cover classes, presented in Tables 2 and 3. The algorithm of Random Forest computes the probability likelihood of the features representing the land cover types over Etosha Pan. This assumes the independence between every pair of pixels and considers the value of cells assigned to each class of the classified satellite image as variables. The implementation of this algorithm in GRASS GIS is performed using r.learn.train module.

Since classification maps invariably contain misclassified pixels and possible classification mistakes, accuracy assessment is an essential step in any RS-based classification. Besides, it enables us to compare the variations of land cover classes. Numerous factors cause possible errors, including the type of input raw data such as Landsat OLI/TIRS; the quality and details of the spectral signatures, the performance of the ML algorithms in processing on pixels in multispectral data and the complexity of the land cover pattern in real landscape mosaic pattern which affect the distinguishability of classes.

The user's accuracy is computed as the number of correctly classified pixels in each land cover class related to total number of reference pixels in ground truth data in the same category. The overall accuracy indicates the total number of accurately classified pixels on the Landsat raster matrix related to the total number of reference pixels. Both overall and user accuracy are indicated in percentage (%) with the best values close to 100%. In contrast, Kappa coefficient is based on the chance-adjusted index of agreement where pixels are randomly assigned to classes and evaluated against the ground truth.

AI/ML framework

In the workflow of AI-driven image processing, the Landsat images are computed by GRASS GIS software which presents a powerful toolset for image analysis. Its excellent and diversified functionality in image processing is reflected in many reported studies which use Earth observation data processed by diverse modules of GRASS GIS.

The signature file for each image was generated using data on spectral signatures which measure the similarity of pixels Digital Numbers (DN) for assignment to classes. This approach was applied to the whole classification process during the MaxLike procedure. We computed the classes using the clustering methods followed by the MaxLike algorithms and got the seed for the next step of the RF algorithm which labelled these pixels assigned to different classes to obtain the classified map in GRASS GIS raster format. The RF function algorithm of ensemble learning was derived from the embedded Python's library of Scikit-Learn and used to test the simulation of the satellite image time series on Etosha Pan, Namibia.

The trained pixels were obtained from the 'RandomForestClassifier' algorithms connected to the Scikit-Learn libraries of Python embedded with GRASS GIS ML function of image analysis. The RF is a type of bagging algorithm of image classification that uses the ML methods of the classification and regression tree decision as learners. The randomness of data points in a raster image evaluated in this algorithm is assessed for reducing model variance. As a result, the advantage of the RF consists in an excellent generalization approach to data classification which combines the results of multiple decision trees to reach a single classification result through anti-overfitting.

RESULTS

The results present the satellite data-driven environmental monitoring of Etosha lake to comprehend seasonal patterns in water availability in the salt lake that affect plant biodiversity in the protected savannah regions in northern Namibia. The AI-driven image analysis revealed that fluctuations in temperature and precipitation played an important role in the water balance over Etosha during autumn days with mixed precipitation (August), maintaining higher relative humidity. This is reflected in vegetation coverage automatically detected on the images. The detailed land cover types are visualized on the map in Figure 4. It shows the variations of vegetation classes which are highly fragmented due to inter-seasonal variations, availability of moisture and actual rainfall situation.

Savannah and grasslands compose the most part of the mosaic in the surrounding landscapes. Higher humidity enables plants to maintain a large amount of leaf area, and to grow during this period.

These two features led to a large capacity of the vegetation to resist droughts, particularly in the late spring period, and to intercept liquid precipitation. Over the past decades, riparian vegetation along an ephemeral lake in Namibia have seen ecological changes. The expansion of salt crust in the summer months and gradual abandonment of the traditional agricultural and fisheries practices and well as landscape dynamics were partly caused by climate (temperature and precipitation) and hydrogeological factors (increase of salt crust). As a result. trends in biodiversity of Etosha seen over the past years are unlikely to persist in the face of climate change. The release of only a small amount of precipitation to the soil eventually contributed to the balanced runoff, sustaining and maintaining local evapotranspiration (ET) with an associated reduction of the sensible heat flux during summer.

Comprehending the decadal effects of the processes of seasonal water cycles in the salt lake is still difficult. The fieldwork data on hydrological monitoring in the Etosha region are scant, and limited. In view of the unavailable hydrological measurements which are not integrated in this study for monitoring saline lakes, the primarily results are obtained from the satellite time-series which are available to evaluate environmental dynamics in salt lake basin. In this regard, integrating space born Landsat data with ecological knowledge on Etosha ecosystems supports hydrological and ecological monitoring of in Namibia. Hence, this work integrated the RS data and ML to obtained the results of the ecological survey of the Etosha landscapes.

The results show a series of maps indicating classified land cover types of the Etosha saline pan based on the time series of satellite images Landsat 8-9 OLI/TIRS. The landscapes and land cover patterns in Namibia are impacted by climate change, which are closely linked to hydrological settings of saline lake through seasonal water cycles. During the evaluated calendar year, the level of water horizon in Etosha experienced dynamics in water level which is visible on the satellite images. In the most shallow areas, water evaporated completely which resulted in intensification of salt crust and expanded area of bare land on the coasts. In contrast, central areas of the lake retained small amount of water which resulted in maintaining the functionality of remaining vegetation, supporting life of wildlife and natural resources. In contrast, grasslands and semi-desert areas experienced restoration and more balanced nature ecosystems compared to the lacustrine environment.

The vegetation declined during the summer months due to the lack of water and high temperatures, which resulted in land desertification in the periods of June to August. Moreover, comparative analysis of the satellite images shows that the expansion of the dry savannah areas, together with the increase of the area of the salt lake and the abandonment of pastures results in low-productivity in the agricultural areas. For example, additionally to natural fauna, fluctuations in water level also constraints agricultural activities of local population that practice agricultural activities in this region. This leads to the abandoned marginal lands and results in habitat homogenization and a reduction in landscape diversity around Etosha lake.

The results shows classified seasonal land cover changes in the Etosha lake and the surrounding landscapes with characteristic features of 10 land cover classes. Figure 4 shows the classification results for different images taken from wet period (March to May) and dry period (June to August) using band combinations of Landsat 8-9 OLI/TIRS.

Using six multi-temporal Landsat images, we evaluated the differences in land cover types in protected region of Etosha lake for environmental monitoring of northern Namibia. After integrating the geospatial data with GRASS GIS, we obtained the results of the performed spatial analysis. The presented thematic maps show ecological differences in the protected saline lake of Namibia for target period of 2022 in the sequence of six months from March to August. The comparison of these regions highlighted areas with the highest land cover changes (coastal parts of the saline lake where water completely dries out during the summer months), and hence, the largest rate of landscape dynamics. The workflow scheme of the GRASS GIS supported results through extracting information of land cover categorization from the classified images.

From a climate-hydrological perspective, this research complements recent evidence on aridity of the Etosha lake which indicates that natural reserves of water in the ephemeral lakes of southern Africa play a key role in dampening heat extremes above the scarce vegetated terrestrial ecosystems such as savannah. It also attributes to saline lake seasonality and cloudiness the role of linkage in the positive feedback between the presence of precipitation and water balance in regions prone to drought such as deserts of Namibia.

The results of the accuracy assessment are presented in the Kappa which shows the discrete multivariate method of accuracy assessment, Table 1.The evaluation of Kappa is acceptable for values above 0.81. The overall classification accuracy was computed above 80% for RF and above 70% for MaxLike which is considered as acceptable in both cases with RF outperforming the classical method, Table 1.

Spatial uncertainty in image classification shows the distribution of pixels to target classes which influences the results of the mapping, Figure 5. It was estimated to avoid bias by the

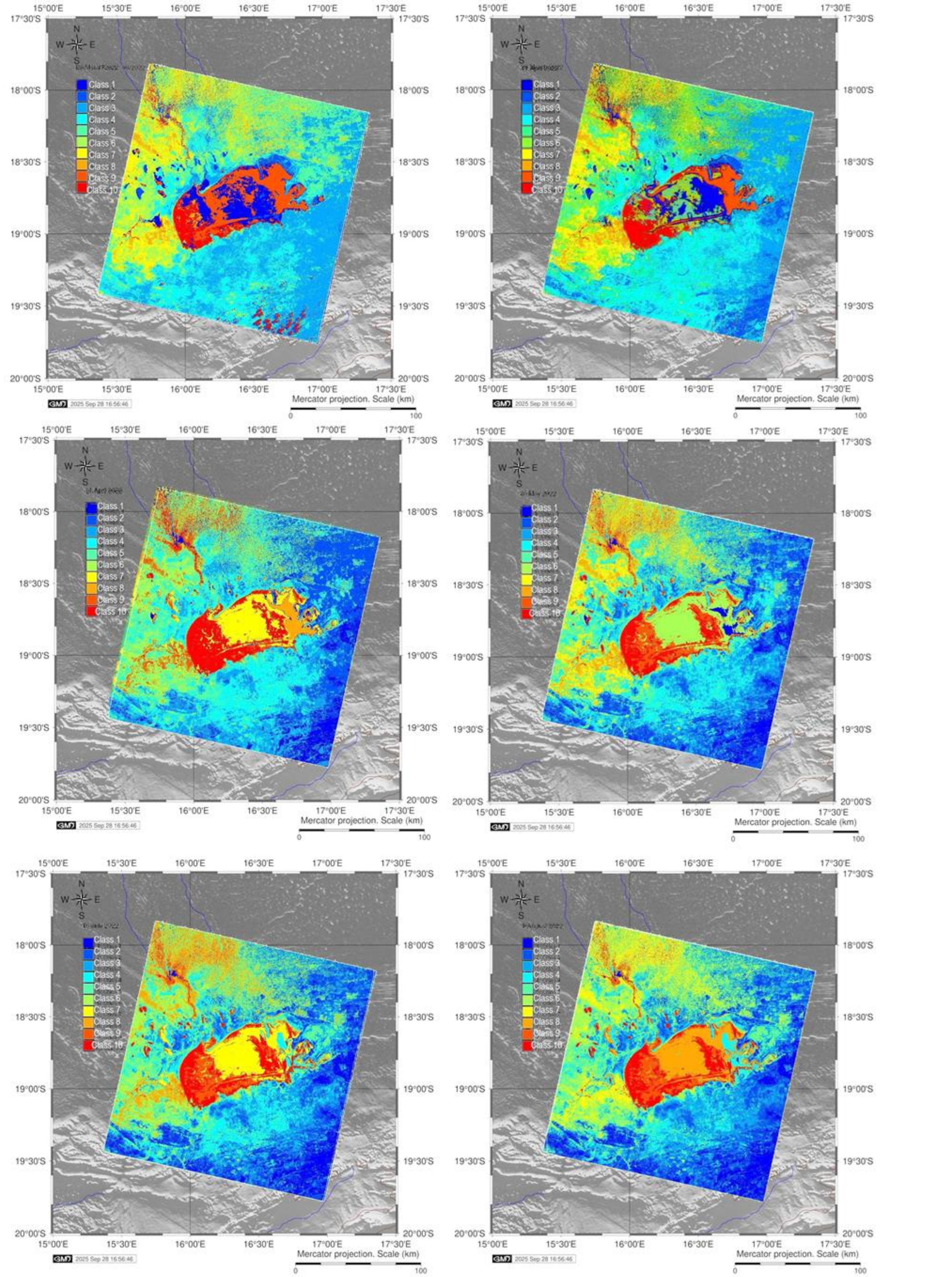

Figure 4. Classified RS data using MaxLike approach in GRASS GIS: (a) March; (b) April; (c) May; (d) June; (e) July; (f) August

Table 1. Estimation of accuracy using Kappa (k) quantification of agreement for six Landsat satellite images processed by Random Forest (RF) and MaxLike algorithms in GRASS GIS. Estimated classes of land cover types for different periods in 2022 over Etosha Pan

Month	Random Forest	Max Like
March	0.82	0.78
April	0.85	0.81
May	0.87	0.85
June	0.81	0.81
July	0.83	0.78
August	0.91	0.81

chi-square test which plots the reject raster map. This map shows the level of threshold which determines the confidence level at which each cell is categorized correctly and accurately assigned to the correct class. In the region over Etosha, 10 distinct land cover types were identified along with their DN codes, number of cells (pixels) in Landsat scenes and their number of training samples for RF validation. The thematic aggregation of classes cannot be directly linked to the parameters of vegetation but provides numerical comparison.

The computational results demonstrated following outcomes. According to the calculated number of pixels corresponding to the cells in the raster images covering the Etosha landscapes, the land use types demonstrated the following changes: 1. Mosaic vegetation and cropland (8.42%), Aquatic or regularly flooded vegetation decreased on 13,59% due to seasonal fluctuations, areas of artificial surfaces declined insignificantly (2.40%),

Mixed broadleaved deciduous forests experienced slight decreased (1.18%), and the class of open grasslands increased to 5.32%. Moreover, rainfed croplands demonstrated stable development with 4.58% of changes, while salt hardpans changed significantly to 12, 73%. Finally, water bodies including Etosha basin decreased significantly due to the seasonal effects (21.73%), Herbaceous vegetation, shrubland and thickets developed relatively stable with minor changes not exceeding 3.25 %, and sparse savannah grasslands occupied similar areas with fluctuations not exceeding 4,72%.

In larger spatial-temporal scale, additional effects of changes in water content over the Etosha lake and associated land cover changes are related to the time influenced by the diurnal water vapor accumulation. For example, the high relative humidity period from afternoon to evening contributes to a larger level of water use efficiency in grass leaves in the shoreline around the lake. This is mostly caused by minimal gradients between the concentrations of intercellular and ambient water vapor levels.

Besides, high variations of humidity over the lake in winter periods cause higher cloudiness at small scales. Since they affect the estimation of evaporation fluxes which include large uncertainties, diurnal changes of water around the lake are difficult to assess and interpret using RS data. The 10 generalized land cover classes include these categories identified using the AI-driven approach: 1. Mosaic vegetation / cropland; 2. Aquatic or regularly flooded vegetation; 3. Bare areas and artificial surfaces; 4. Mixed broadleaved deciduous forests; 5. Open grassland; 6. Rainfed cropland; 7. Salt hardpans; 8. Water bodies (Etosha basin and other lakes); 9. Herbaceous vegetation, shrubland and thickets; 10. Sparse savannah grasslands.

The effects of several AI approaches in geospatial data analysis were investigated using GRASS GIS. Specifically, image processing and classification were performed using embedded Python libraries, including algorithms of maximal likelihood (MaxLike), random forest (RF) and other ML methods. The computed class means of Digital Numbers (DN) of pixels assigned to 10 land cover classes in landscapes of Etosha Pan are shown in Table 2. It shows each multispectral band (1 to 7) of Landsat 8-9 OLI/TIRS from March to August 2022.

The ML-based image processing revealed fluctuations in the salinization of the Etosha Pan which is caused by seasonal changes from dry to wet periods. During hot summertime, rains gradually slow and cease leaving the basin of the lake covered by crust of salt and minerals. Parched brownish landscapes in the western and central parts of lake clearly contrast with the remaining segments of the lake still filled with water. Such changes are visible in the images where different colours of water varying from electric cyan to dark navy blue show the depths of the lake with darker shadows indicating deeper segments.

The difference between water input in rainy periods (spring-winter) and dry periods of droughts (summer and early autumn) forms effects on water output as evapotranspiration and water discharge, plus the variation in the soil water content which reflects the aridity during droughts. Though direct measurements have not been included in estimation of the past water balance, our study revealed the effectiveness of RS data and ML techniques for evaluation of water-salt variations in Etosha. Combined with data on rainfall periods in the same calendar years, such as seasonal periods of mixed precipitation, contributed to higher throughfall, which in turn contributes to higher net precipitation (soil water recharge, in absence of runoff) and evaporative conditions inside the ephemeral lake of Etosha.

In the set of false and natural colour composites of images, the bright colours of the remaining water and a thin channel connecting the deep part of the basin with drying segment filled with salt and minerals offers a clear contrast with the parched brownish landscapes of savannah of the surroundings. In the dry months (June to August) the bare soil areas contrast with the images in the wet season (March to May) with areas covered by lush vegetation. The traditional pixel-based and object-based approaches were compared to detect the best methods of feature extraction for classification. The classes were more easily segmented compared to the areas with similar parameters such as class 'sparse savannah grasslands' compared to class 'herbaceous vegetation, shrubland and thickets'. Furthermore, the RF techniques consider spectral properties of data obtained from diverse sensors such as surface forms, texture of land parcels, topology and pattern heterogeneity.

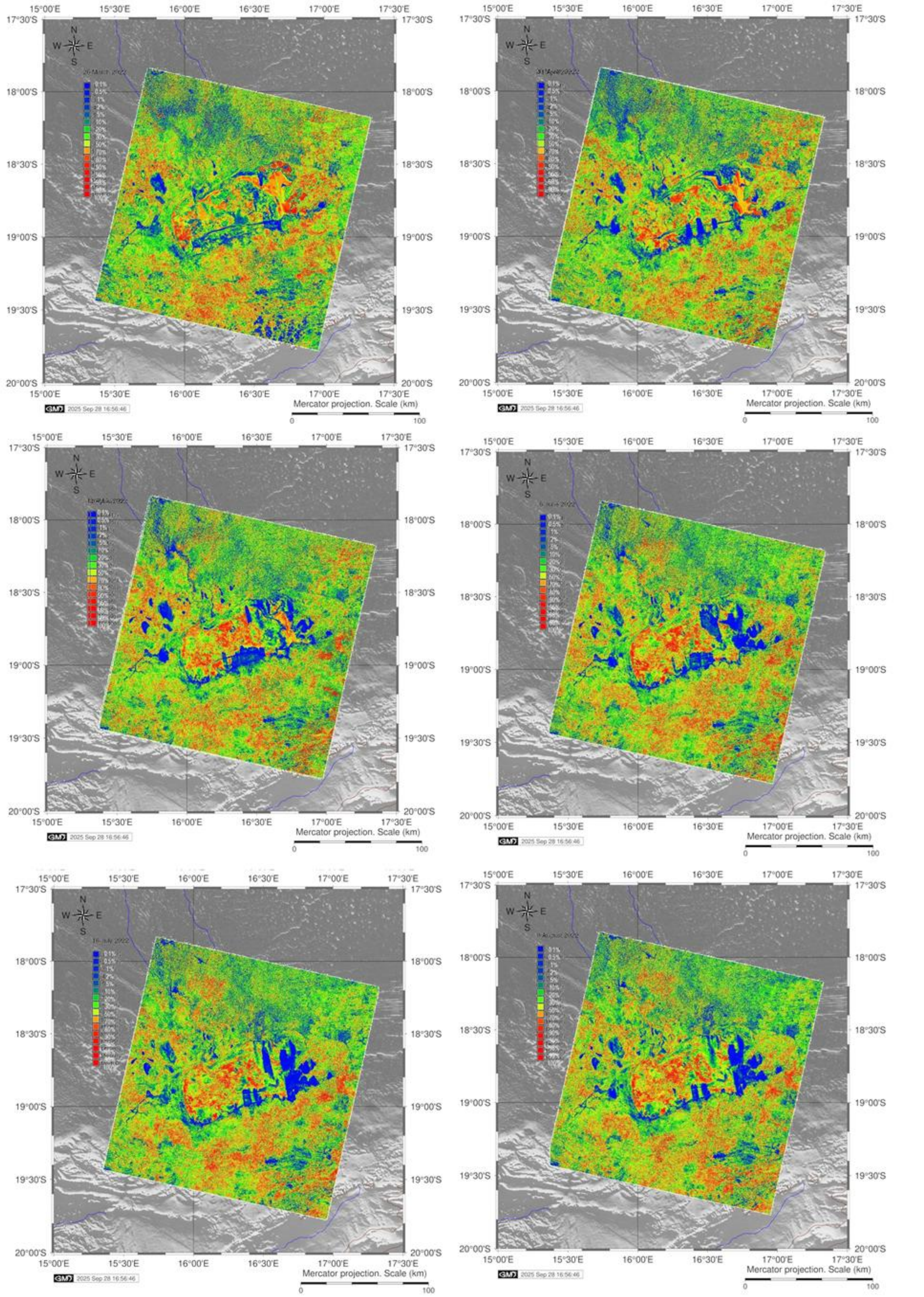

Figure 5. Maps of accuracy assessment showing rejection probability of the misclassified pixels in percentage (%): (a) March; (b) April; (c) May; (d) June; (e) July; (f) August

Table 2. Computed class means of Digital Numbers (DN) of pixels computed for pixels assigned to 10 land cover classes in landscapes of Etosha Pan within each multispectral band (1 to 7) of Landsat 8-9 OLI/TIRS for period March, April and May (left) and June, July and August (right) of 2022

Class	Band 1	Band 2	Band 3	Band 4	Band 5	Band 6	Band 7
2022: March							
1	8098.62	8512.65	8631.06	7546.23	7267.76	7546.9	7557.35
2	7553.06	7632.71	8068.18	7839.98	12844.7	10069.7	8585.51
3	7777.81	7884.66	8495.97	8214.02	15113.7	11568.1	9364.32
4	7877.98	7975.17	8689.92	8307.54	17252	12569.4	9727.25
5	7897.2	8012.3	8915.56	8403.3	19960.2	13680.2	10132.2
6	8411.29	8626.87	9550.21	9501.78	16952.6	14944.5	11811.4
7	8301.92	8521.3	9721.61	9335.65	20995.1	15866.2	11783.2
8	8916.74	9267.16	10375	10898.8	14101.7	15346.2	13192.6
9	9214.32	9617.25	10915.6	11471.1	16763.6	17559.3	14612.4
10	10372.2	11077.1	13007	14103.9	17708.2	20050.3	17456.2
2022: April							
1	9172.27	9666.92	11061.3	12392.3	14007.9	16706.8	15588.5
2	9727.84	10277.6	11940.7	13629.7	15604.9	19417.9	17995.7
3	10168.7	10794.8	12759.1	14845.5	17051.6	21189	19595
4	10779.8	11499.7	13878.3	16423.6	18753.7	22650.5	20923.9
5	11444.7	12242.6	15038.4	18017.7	20503.9	24315.4	22337.3
6	12047.4	12943.1	16145.8	19523	22077.2	25880.5	23886.3
7	12259.9	13241.8	16912	20767	23376.4	27664.4	25777
8	12268.5	13409.6	17712.3	22303.6	25270	29699	27773.2
9	12286.8	13596.3	18865.7	24514.6	28062.5	32565.3	30349.5
10	12888.2	14353.3	20060.4	26171.5	29941.7	34355.6	32069.7
2022: May							
1	8111.51	8199.08	8100.88	7465.42	7287.35	7335.55	7330.84
2	7565.9	7794.02	8480.23	8399.37	13105.3	11135.9	9540.2
3	7941.53	8209.27	9135.12	9131.33	14663.5	13138.1	10966.2
4	8278.6	8635.24	9757.47	10183.6	14710.6	15182	12997.8
5	8007.61	8238.4	9379.12	9007.12	18137.6	13349.7	10649.6
6	7959.3	8113.15	9263.84	8488.51	22413.9	12764.6	9831.97
7	8460.35	8799.31	10364.7	10092.9	20827.9	15638.7	12351.6
8	8552.87	8939.44	10306.6	10660.9	17349.2	16382.3	13624.4
9	8999.75	9517.87	11173.8	12159.9	17889.8	18838.8	16259.8
10	10309.3	11076.4	13413.5	15174.4	20565.5	22691.1	20127.9

Class	Band 1	Band 2	Band 3	Band 4	Band 5	Band 6	Band 7
2022: June							
1	7399.11	7700.46	8093.33	7507.22	7510.31	7816.17	7813.15
2	7959.95	8136.6	8833.45	8718.96	13723.5	11931.4	9971.79
3	8201.19	8373.2	9271.63	8957.59	15874.8	13059	10480
4	8508.25	8772.75	9770.7	9832.82	16037.3	15151	12167.9
5	9122.23	9558.15	10904.5	11408.6	16780.3	17255.5	14327.4
6	8273.09	8469.63	9647.99	9097.73	19055.1	13632	10670.7
7	8723.8	9047.95	10477.3	10227.1	19679.1	15727.3	12388
8	8183.4	8340.86	9546.97	8750.16	22739.3	13310.2	10176.4
9	10457.7	11207.5	13337.1	14292.3	18851.1	19633.9	17061.3
10	19323.2	20808	24156	26234.2	25164.8	10514.2	9812.97
2022: July							
1	7033.1	7688.66	8510.3	8449.8	7990.8	8203	7274
2	7560.4	8281.7	8560.3	8224.9	13040.9	11089.2	9779.6
3	8216.2	8939.2	9712.9	8334.1	15433.2	14969.2	10943.7
4	7644.4	7384.1	8481	8648.1	16999.2	16562.3	13553.5
5	10656	9420.3	10772.2	11487.4	16169.5	17778	14108.5
6	9307.7	9169.1	9759	9509.2	9315.2	18022.2	10479.6
7	9608.7	9393.8	10979.8	10170.6	20216.8	15145.9	10732.8
8	8261.8	8162.6	9058.5	8295.3	24431.1	13640.4	10337.6
9	11175.6	12129.1	16335.5	22089.8	25585	11287	19048.6
10	19820.4	20904.1	24044.4	26760.4	25635.7	10727.8	9325.1
2022: August							
1	7041.39	7881.47	8779.5	8671.9	8448.1	8012.5	7620.7
2	7509.45	8198	8426.4	8006.5	13539.5	11770.2	10881.2
3	10167	10929.8	13643.9	17182.6	19783.6	24339.5	20655.8
4	10120.6	10907.8	13742.9	17641.8	21205.1	26004.9	22347.9
5	10729.5	11682.5	14818.6	18738.2	22049	26015.7	21883
6	10332.3	11175.8	14259.5	18477.3	22424	27292.5	23640.7
7	11140.5	12116.5	15589.2	19917.4	23254.2	27496.6	23605
8	10528.9	11417.4	14751.7	19200.1	23303.7	28395.3	24923.8
9	10891.9	11843.6	15584.2	10448.8	14362.9	19302.3	16023.8
10	12081.2	20117.6	24961.7	26527.8	24521.1	10527	9580.5

AI technologies integrated in cartographic workflow enable to process and analysis complex landscape patterns in diversified environmental regions. In view of this, the use of the ML by GRASS GIS is considered a key step in the development of cartographic tools of the RS data processing. Therefore, the distributions of pixels according to spectral reflectance alone could only discriminate those regions that have distinct characteristics of brightness and spectral reflectance. The comparison of the results enabled us to optimize image processing workflow using a series of GRASS GIS modules including the ML components integrated with Scikit-Learn package of Python.

The distribution of spectral characteristics of diverse land cover types is affected by seasonal changes which are integrated with the effects from salinization of the basin in dry periods from May onwards. Thus, the performance of RF was further evaluated with several processed images. Thus, the ML model was trained, and its performance was investigated using a non-random data partition approach of image classification. Instead of doing random data partition which splits image into segments, the RF algorithm organized raster image into different groups of classes according to the land cover types around Etosha and then divided each scene using previously done training dataset obtained from the unsupervised automatic classification by clustering. Major research results can be summarized in the following highlights:

- Seasonal oscillations in water / salt level in saline Etosha Pan were identified using AI-driven geospatial data: visualized and analyzed Landsat 8-9 OLI/TIRS images.
- Scripting techniques of GRASS GIS for image processing is used to visualize spatial variability of landscapes in Namibia.

Compared to the performance of 'MaxLike' classification, RF classified performed better in case of similar classes in terms of separability of adjacent landscape patches. For instance, the grasslands, salt hardpan area of Etosha and flooded areas clearly distinct from the mosaic trees and regions of broadleaved deciduous forests due to the different texture characteristics and spectral reflectance of pixels. The outperformance of the RF Classifier consists in its nature of supervised learning algorithm. It is considered among one of the most intuitive classifiers which implies the probabilistic approach and normal distribution of the data and straightforward implementation.

The likelihood of the pixels assigned to each land cover class during image partition which partitions the pixels in the images according to the decision rule which evaluates the suitability of pixels into a target class of land cover types.

Moreover, RF demonstrated the compatible advancements in methodological workflow compared to other advanced ML techniques such as Convolutional Neural Networks (CNN). Thus, based on the benchmarking against the CNN state-of-the-art approaches that are also used in RS data processing, RF presents the ensemble of decision trees. It is well-suited for tabular data and tasks that require interpretability and information retrieval. Contrary to RF, the CNNs is a type of neural network that is particularly effective for image and audio processing with hierarchical features identification.

Overall, the results of RF classification using ensemble learning approach are more satisfying compared to the unsupervised classification despite the occasional pixels misclassification in some regions of central basin where over-fragmented mosaic of patches are visible. The relevance of the interception capacity of water by plants around Etosha Pan was particularly high during early spring (March). In this case, the liquid water was used to refill the canopy and soil reservoirs, without being lost as runoff. The identification of the satellite images demonstrated large areas covered by grass and savannah, which represents most of the precipitation in the early spring period and August. This indicated the process of water interception by leaves and vegetation, which is emitted during evaporation processes locally.

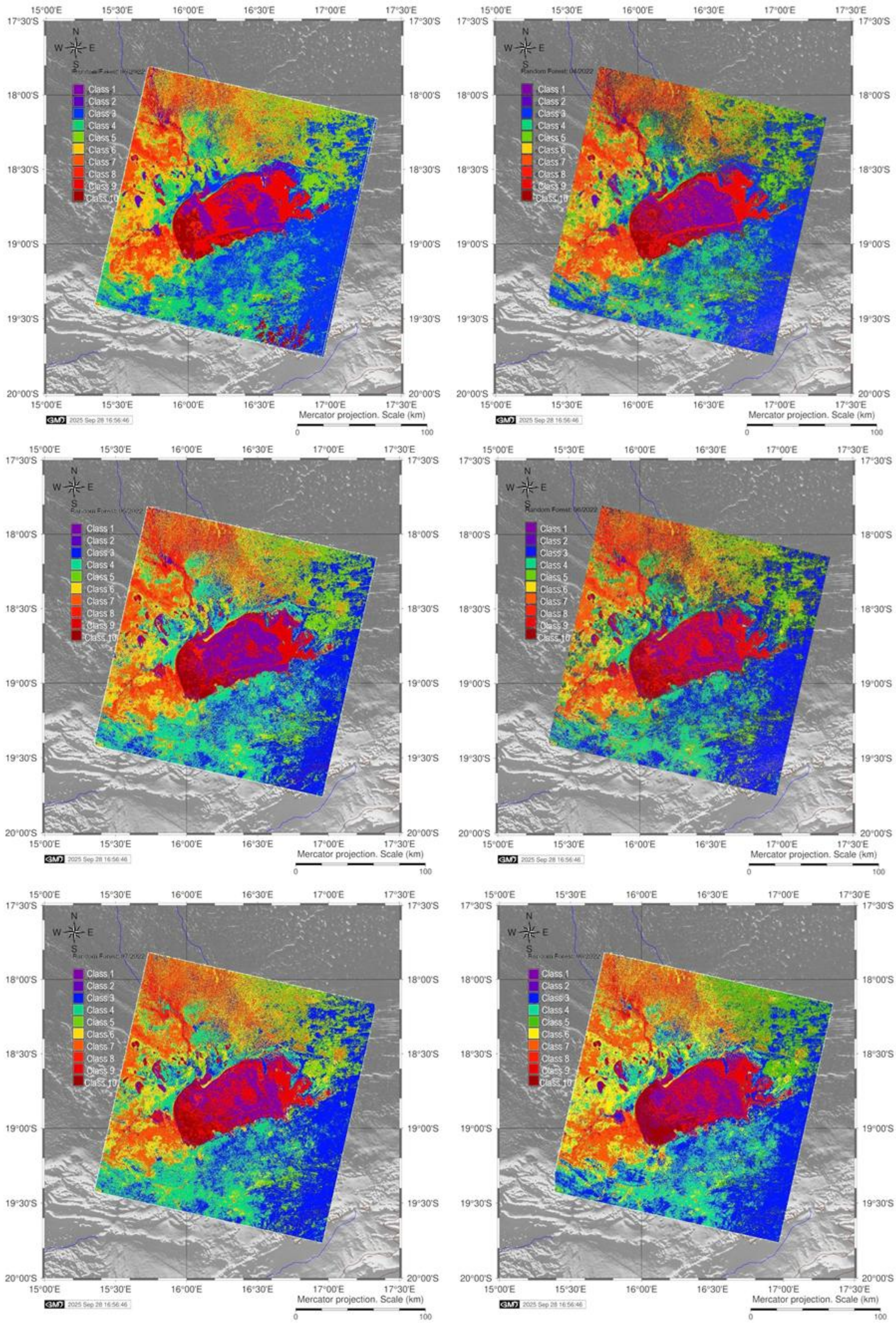

Figure 6. AI-driven classification of satellite images: a case of Random Forest: (a) March; (b) April; (c) May; (d) June; (e) July; (f) August

The responses of vegetation to eco-hydrological processes are detected as changes in land cover types on the time series of the satellite images. Technically, the ensemble learning approach is based on the adaptive integrating of land cover features based on automated recognition of spectral properties of pixels constituting raster scenes. The presented RS-based maps show large spatial heterogeneity in the evolution of desert, salt lake and vegetation areas around Etosha Pan in the assessed short-term one-year calendar year period from March to August in 2022. Here, we evaluated the technical methods of AI-driven image processing in order to select the optimal approach. The use of the RF algorithm had the best performance with Landsat image processing compared to other ML models and MaxLike, as it accurately depicts spatial occupation of savannah vegetation and salt lake areas through optimal pixel transformation that determines the boundaries between cell points based on predefined classes.

DISCUSSION

Satellite images as a major type of RS data provide excellent source of information for Earth observation. Such data are widely used and their applications are discussed in the relevant literature on RS-based environmental monitoring and mapping [57-59]. The key to successfully extract information from the RS data for thematic mapping is the methods of image processing that performs analysis of raster scenes through classification, segmentation, enhancing the spectral contrasts between visible objects and other techniques. Machine-based interpretation of the extracted information ensures identification of the objects visible on the Earth's surface. The question is how to efficiently, accurately and automatically detect and recognize those objects for cartographic visualization.

The developed algorithms of the AI-based image analysis support narratives to interpret biodiversity changes and environmental monitoring of southern African landscapes. In this way, AI-driven technologies enable us to identify habitats and to develop narratives for interpreting land cover changes. This project demonstrated the use of the Geospatial Artificial Intelligence (GeoAI) in RS data processing for mapping. We focused on the Land Use and Land Cover (LULC) in selected landscapes of Namibia. LULC detection and mapping is important for understanding human-climate-environmental interactions through cartographic monitoring. Accurate LULC mapping is possible using integrated data-driven approach that combines RS data and GeoAI models.

Examples of GeoAI, such as Deep Learning (DL), convolutional neural networks (CNN) and ML techniques such as RF, SVM, Naive Bayes, Gradient boosting, enhances the precision of LULC mapping through advanced level of image analysis [60-62]. Besides, scripting techniques of Python and R libraries significantly facilitate the workflow to increase the speed of time series analysis. As a result, the combination of Python scripts and ML/DL algorithms significantly improves the quality of satellite image processing for environmental monitoring.

Landscapes represent land surface where environmental processes interplay to provide habitat and resources for life. Cumulative effects from climate change, biophysical and anthropogenic processes affect landscapes and cause land cover changes, decline of vegetation and ecosystem degradation. Such issues are visible on spaceborne RS data and can be detected for operative environmental monitoring using GeoAI tools. In this study we identified changes in land cover types around Etosha lake, north Namibia, using time series of satellite images. The maps of spatio-temporal vegetation dynamics and changes in land cover types were prepared using open source RS data. In future studies, additional measurements at the soil level can be performed in the subsequent years to evaluate the dynamics, in which the soil moisture around the lake can be measured for environmental prognosis. Moreover, water discharge can be measured at the catchment level subject to the availability of fieldwork and compared to the total evapotranspiration available from the general climate databases on Namibia. This would enable us to examine the variability of the transpiration levels and their effects on land cover types for one year.

Water balance regulates meteorological conditions and maintains humidity, thus playing the role of buffer for the ecosystem. Since there are few studies dealing with the contribution of saline ephemeral lakes on the ecosystems of southern Africa and the changes in land cover types to the water balance, this work has contributed to filling in this gap with a case of south-western region of Africa. Further implications of this work include predicting the impact of different climate change scenarios in southern regions of Africa. Specifically, this study contributes to understanding vegetation distribution around Etosha Pan, combining environmental vulnerability and exposure to possible future climate change to identify areas at greatest risk of vegetation change in Namibia, southern Africa.

Land cover changes in Namibia reflect regional environmental dynamics in southern Africa which is subject to climate change [63-64]. The biodiversity in Etosha lake strongly depends on water availability and complex issues of hydrological cycles of this saline lake [65]. Hence, ecosystems and hydrogeology of the saline lake present interconnected environmental problems for southern African environment [66]. Together with specific geomorphology of desert that induce sand dust storms, water scarcity poses a threat to the ecological sustainability and resilience of the landscapes in southern Africa [67]. Addressing these critical issues is one of the most challenging tasks in Earth sciences, because African landscapes are crucial for the global environmental sustainability [68]. Given the vital role that nature conservation plays for protecting landscapes, it is essential to perform Earth observation using methods of GIS and remote sensing data. Since methodological capacities of GIS are technically limited, this study extended this approach through machine learning (ML). Using ML, temporal dynamics of the Etosha saline lake, northern Namibia, was evaluated through comparative analysis of satellite images taken in different periods. This enabled to reveal changes in water availability in lake which is essential for wildlife functionality in the environment of Etosha lake.

CONCLUSION

The paper contributes to the development of environmental monitoring aimed at adaptation of Namibia to climate change – as one of the aims of the project is to understand, in a spatial-explicit manner, which are risks associated to climate change of unique protected landscapes of Etosha Pan and surroundings. Besides, the AI-driven mapping of Namibia is presented for protection and restoration of biodiversity and ecosystems in southern Africa as the project is aiming at environmental monitoring. Finally, times series of the satellite images was analysed for better understanding of vegetation distribution in the protected areas of Namibia. This enables identification of the climate-environmental pressures that caused environmental changes in habitats and biodiversity.

This study demonstrated advanced application of the geospatial AI tools for monitoring landscapes in Namibia. The use of ML methods for RS data processing enabled to reveal landscape dynamics in Etosha salt lake region. The ML-generated maps of land cover types which support better understanding of the distribution of diverse landscape patterns over the country and plant diversity. The functionality of the ML and AI tools of GRASS GIS and their applicability in RS data processing was evaluated with regard to classification of multispectral satellite images. A motivation of this study was to perform the AI-supported environmental analysis of the Etosha salt pan, northern Namibia, with the aim to explore the climatic and seasonal factors that affect water availability in the basin.

DATA AVAILABILITY STATEMENT

The authors confirm that the data that supports the findings of this study are available within the article. Raw data that support the finding of this study are available from the corresponding author, upon reasonable request.

CONFLICT OF INTEREST

The authors declare that there are no conflict of interest with any individual, institution, or organization in the preparation, evaluation, or publication of this study.

USE OF AI FOR WRITING ASSISTANCE

Not declared.

ETHICS

There are no ethical issues with the publication of this manuscript.

REFERENCES

[1]. V. Patil, Z. S. N., R. Bhosale, N. Shetty and V. Shah, "Land Cover Mapping Using Semantic Segmentation Models," 2023 7th International Conference On Computing, Communication, Control And Automation (ICCUBEA), Pune, India, 2023, pp. 1-5, doi: 10.1109/ICCUBEA58933.2023.10392136.

[2]. M. Klaučo, B. Gregorová, U. Stankov, V. Marković, P. Lemenkova, "Determination of ecological significance based on geostatistical assessment: a case study from the Slovak Natura 2000 protected area", *Central European Journal of Geography*, Vol. 5, 28–42, 2013.

[3]. P. Lemenkova (2022). Evapotranspiration, vapour pressure and climatic water deficit in Ethiopia mapped using GMT and TerraClimate dataset. Journal of Water and Land Development, 54(7-9), 201--209. 10.24425/jwld.2022.141573

[4]. S. Xiang, Q. Xie and M. Wang, "Semantic Segmentation for Remote Sensing Images Based on Adaptive Feature Selection Network," in *IEEE Geoscience and Remote Sensing Letters*, vol. 19, pp. 1-5, 2022, Art no. 8006705, doi: 10.1109/LGRS.2021.3049125

[5]. M. Klaučo, B. Gregorová, P. Koleda, U. Stankov, V. Marković, P. Lemenkova, "Land Planning as a Support for Sustainable Development Based on Tourism: A Case Study of Slovak Rural Region", *Environmental Engineering and Management Journal*, Vol. 16(2), 449–458, 2017.

[6]. Lemenkova, P. (2023). A GRASS GIS Scripting Framework for Monitoring Changes in the Ephemeral Salt Lakes of Chotts Melrhir and Merouane, Algeria. *Applied System Innovation*, *6*(4), 61. https://doi.org/10.3390/asi6040061

[7]. P. Lemenkova, 2025. Machine Learning Methods of Remote Sensing Data Processing for Mapping Salt Pan Crust Dynamics in Sebkha de Ndrhamcha, Mauritania, Artificial Satellites, 60(2), 37--69. doi: 10.2478/arsa-2025-0003

[8]. G. Thiyagarajan and V. Vijayalakshmi, "Classification of Land Cover using Machine Learning Models in Landsat Satellite Data," 2024 15th International Conference on Computing Communication and Networking Technologies (ICCCNT), Kamand, India, 2024, pp. 1-6, doi: 10.1109/ICCCNT61001.2024.10725490.

[9]. F. Yasmin, A. H. M. Sarowar Sattar and M. Kumar Paul, "Water Bodies Identification in Landsat 8 OLI Image Using Machine Learning," *2019 22nd International Conference on Computer and Information Technology (ICCIT)*, Dhaka, Bangladesh, 2019, pp. 1-6, doi: 10.1109/ICCIT48885.2019.9038562.

[10]. A. V. Kakade, S. Rajkumar, K. Suganthi, L. Ramanathan, "Object Detection in Satellite Images Using Modified Pyramid Scene Parsing Networks," in *Sensor Data Analysis and Management: The Role of Deep Learning*, IEEE, 2021, pp.147-160, doi: 10.1002/9781119682806.ch9.

[11]. Q. Safder, H. Zhang and Z. Zheng, "Burnt Area Segmentation with Densely Layered Capsules," *IGARSS 2022 - 2022 IEEE International Geoscience and Remote Sensing Symposium*, Kuala Lumpur, Malaysia, 2022, pp. 2199-2202, doi: 10.1109/IGARSS46834.2022.9884323.

[12]. D. R. Rao, S. Noorjahan and S. A. Fathima, "Classification of Land Cover Usage from Satellite Images using Deep Learning Algorithms," *2022 International Conference on Electronics and Renewable Systems (ICEARS)*, Tuticorin, India, 2022, pp. 1302-1308, doi: 10.1109/ICEARS53579.2022.9752282.

[13]. Z. Benbahria, M. F. Smiej, I. Sebari and H. Hajji, "Land cover intelligent mapping using transfer learning and semantic segmentation," *2019 7th Mediterranean Congress of Telecommunications (CMT)*, Fez, Morocco, 2019, pp. 1-5, doi: 10.1109/CMT.2019.8931403.

[14]. Z. Liu, X. Liu, M. Yu and X. Yang, "DMAM-UNET:An Improved Unet Semantic Segmentation for Water Body Extraction from Remotely Sensed Image," *IGARSS 2023 - 2023 IEEE International Geoscience and Remote Sensing Symposium*, Pasadena, CA, USA, 2023, pp. 3726-3729, doi: 10.1109/IGARSS52108.2023.10283313.

[15]. V. Poliyapram, N. Imamoglu and R. Nakamura, "Deep Learning Model for Water/Ice/Land Classification Using Large-Scale Medium Resolution Satellite Images," *IGARSS 2019 - 2019 IEEE International Geoscience and Remote Sensing Symposium*, Yokohama, Japan, 2019, pp. 3884-3887, doi: 10.1109/IGARSS.2019.8900323.

[16]. A. Shalan, K. Tarmissi and N. A. Walee, "Vulnerability Analysis and Quality Improvement of Early Wildfire Detection Datasets for Machine-Learning Applications," *2024 IEEE 13th International Conference on Communication Systems and Network Technologies (CSNT)*, Jabalpur, India, 2024, pp. 754-760, doi: 10.1109/CSNT60213.2024.10546223.

[17]. Monali Gulhane; Sandeep Kumar, "Oriental Method to Predict Land Cover and Land Usage Using Keras with VGG16 for Image Recognition," in *Advances in Aerial Sensing and Imaging*, Wiley, 2024, pp.33-46, doi: 10.1002/9781394175512.ch2.

[18]. Z. Tang, X. Luo, Z. Yan, S. Li, S. Xiao and H. Li, "An Automatic Sample Augmentation Method for Paddy Rice

Mapping Based on Segment Anything Model and Phenological Features—A Case Study in Southwest China," in *IEEE Journal of Selected Topics in Applied Earth Observations and Remote Sensing*, doi: 10.1109/JSTARS.2025.3606650.

[19]. P. Lemenkova, (2025). Machine Learning Algorithms of Remote Sensing Data Processing for Mapping Changes in Land Cover Types over Central Apennines, Italy, Journal of Imaging, 11(5), 153. 10.3390/jimaging11050153

[20]. Lemenkova, P. (2025). Improving Bimonthly Landscape Monitoring in Morocco, North Africa, by Integrating Machine Learning with GRASS GIS. *Geomatics*, *5*(1), 5. https://doi.org/10.3390/geomatics5010005

[21]. A. Cuartero, M. E. Paoletti, A. R. Presas and J. M. Haut, "Bi-Dimensional Vector Data Analysis of Positional Accuracy of Landsat-8 Image with Pycircularstats," *IGARSS 2022 - 2022 IEEE International Geoscience and Remote Sensing Symposium*, Kuala Lumpur, Malaysia, 2022, pp. 2442-2445, doi: 10.1109/IGARSS46834.2022.9883588

[22]. P. Lemenkova, 2025. Mapping Woodlands in Angola, Tropical Africa: Calculation of Vegetation Indices From Remote Sensing Data. Agriculture and Forestry, 70(3), 185–202. 10.17707/AgricultForest.70.3.13

[23]. N. Dinh Duong, "Decomposition of Landsat 8 OLI Images by Simplified Spectral Patterns for Land Cover Mapping," *2018 10th IAPR Workshop on Pattern Recognition in Remote Sensing (PRRS)*, Beijing, China, 2018, pp. 1-13, doi: 10.1109/PRRS.2018.8486245.

[24]. Chunhong Pan, Gang Wu, V. Prinet, Qing Yang and Songde Ma, "A band-weighted landuse classification method for multispectral images," *2005 IEEE Computer Society Conference on Computer Vision and Pattern Recognition (CVPR'05)*, San Diego, CA, USA, 2005, pp. 96-102 vol. 1, doi: 10.1109/CVPR.2005.14.

[25]. M. Clements, and R. Washington, "Summer Dust Emissions From the Etosha Pan, Namibia: The Role of the Namib Anabatic-Sea Breeze System", *Journal of Geophysical Research: Atmospheres*, Vol. 128, e2022JD036815, 2023.

[26]. R. I. Matichuk, P. R. Colarco, J. A. Smith, O. B. Toon, "Modeling the transport and optical properties of smoke aerosols from African savanna fires during the Southern African Regional Science Initiative campaign (SAFARI 2000)", *Journal of Geophysical Research: Atmospheres*, Vol. 112, 2007.

[27]. G. F. S. Wiggs, M. C. Baddock, D. S. G. Thomas, R. Washington, J. M. Nield, S. Engelstaedter, R. G. Bryant, F. D. Eckardt, J. R. C. von Holdt, S. Kötting, "Quantifying Mechanisms of Aeolian Dust Emission: Field Measurements at Etosha Pan, Namibia", *Journal of Geophysical Research: Earth Surface*, Vol. 127, e2022JF006675, 2022.

[28]. M. R. Jury, E. Brunke, and M. Schormann, "Aircraft section measurements of meteorology and ozone in northern Namibia during SAFARI-92", *Journal of Geophysical Research: Atmospheres*, Vol. 101, 23713–23720, 1996.

[29]. N. M. Mahowald, R. G. Bryant, J. del Corral, L. Steinberger, "Ephemeral lakes and desert dust sources", Geophysical Research Letters, Vol. 30, 2003.

[30]. M. Clements, R. Washington, Atmospheric Controls on Mineral Dust Emission From the Etosha Pan, Namibia: Observations From the CLARIFY-2016 Field Campaign. Journal of Geophysical Research: Atmospheres, Vol. 126, e2021JD034746, 2021.

[31]. V. E. Fox, P. M. Lindeque, R. E. Simmons, H. H. Berry, C. Brain, R. Brabys, "Flamingo 'rescue' in Etosha National Park, 1994: technical, conservation and economic considerations", Ostrich, Vol. 68, 72–76, 1997.

[32]. B. Parasharya, D. Rank, D. M. Harper, G. Crosa, S. Zaccara, N. Patel, C. Joshi, "Long-distance dispersal capability of Lesser Flamingo Phoeniconaias minor between India and Africa: genetic inferences for future conservation plans", Ostrich, Vol. 86(3), 221–229, 2015.

[33]. F. H. Neumann, M. K. Bamford, "Shaping of modern southern African biomes: Neogene vegetation and climate changes", Transactions of the Royal Society of South Africa, Vol. 70(3), 195–212, 2015.

[34]. B. E. Morgan, D. T., Bolger, J. W. Chipman, J. T. Dietrich, "Lateral and longitudinal distribution of riparian vegetation along an ephemeral river in Namibia using remote sensing techniques", *Journal of Arid Environments*, Vol. 181, 104220, 2020.

[35]. R. Van Aarde, Y. De Beer, R. Guldemond, "Elephants, drought and the woody vegetation in Namibia's Etosha National Park", *Transactions of the Royal Society of South Africa*, Vol. 59(2), 123, 2004.

[36]. D. H. M. Cumming, M. B. Fenton, I. L. Rautenbach, R. D. Taylor, G. S. Cumming, M. S. Cumming, J. M. Dunlop, A. G. Ford, M. D. Hovorka, D. S. Johnston, M. Kalcounis, Z. Mahlangu, and C. V. R. Portfors, "Elephants, woodlands and biodiversity in southern Africa", *South African Journal of Science*, Vol. 93, 231–236, 1997.

[37]. D. Western, D. Maitumo, "Woodland loss and restoration in a savanna park: a 20-year experiment", *African Journal of Ecology*, Vol. 42, 111–121, 2004.

[38]. E. Gargallo, "Community Conservation and Land Use in Namibia: Visions, Expectations and Realities", *Journal of Southern African Studies*, Vol. 46(1), 129–147, 2020.

[39]. P. Lemenkova, "Monitoring Seasonal Fluctuations in Saline Lakes of Tunisia Using Earth Observation Data Processed by GRASS GIS", *Land*, Vol. 12(11), 1995, 2023.

[40]. J. M. Melack, "Ecological dynamics in saline lakes", *SIL Proceedings*, Vol. 1922-2010, 28(1), 29–40, 2002.

[41]. P. Lemenkova, 2022. Mapping Climate Parameters over the Territory of Botswana Using GMT and Gridded Surface Data from TerraClimate. ISPRS International Journal of Geo-Information, 11(9), 473, 10.3390/ijgi11090473

[42]. L. Krienitz, C. Bock, K. Kotut, W. Luo, "Picocystis salinarum (Chlorophyta) in saline lakes and hot springs of East Africa", *Phycologia*, Vol. 51(1), 22–32, 2012.

[43]. S. Trigg, S. Flasse, "Characterizing the spectral-temporal response of burned savannah using in situ spectroradiometry and infrared thermometry", *International Journal of Remote Sensing*, Vol. 21(16), 3161–3168, 2000.

[44]. H. Wagenseil, C. Samimi, "Assessing spatio-temporal variations in plant phenology using Fourier analysis on NDVI time series: results from a dry savannah environment in Namibia", *International Journal of Remote Sensing,* Vol. 27(16), 3455–3471, 2006.

[45]. P. Lemenkova, "Deep Learning Methods of Satellite Image Processing for Monitoring of Flood Dynamics in the Ganges Delta, Bangladesh", *Water*, Vol. 16(8), 1141, 2024a.

[46]. Z. Huang, B. Lees, "Representing and reducing error in natural resource classification using model combination", *International Journal of Geographical Information Science*, Vol. 19(5), 603–621, 2005.

[47]. P. Lemenkova, "Artificial Intelligence for Computational Remote Sensing: Quantifying Patterns of Land Cover

Types around Cheetham Wetlands, Port Phillip Bay, Australia", *Journal of Marine Science and Engineering*, Vol. 12(8), 1279, 2024b.

[48]. D. P. Roy, J. Ju, C. Mbow, P. Frost, T. Loveland, "Accessing free Landsat data via the Internet: Africa's challenge", *Remote Sensing Letters*, Vol. 1(2), 111–117, 2010.

[49]. P. Lemenkova, "Image Segmentation of the Sudd Wetlands in South Sudan for Environmental Analytics by GRASS GIS Scripts", *Analytics,* Vol. 2(3), 745-780, 2023a.

[50]. P. Lemenkova, "Using open-source software GRASS GIS for analysis of the environmental patterns in Lake Chad, Central Africa", *Die Bodenkultur Journal of Land Management Food and Environment,* Vol. 74(1), 49-64, 2023b.

[51]. T. S. Shahfahad, M. W Naikoo, A. Rahman, A. S. Gagnon, A. R. M. T. Islam, and A. Mosavi, "Comparative evaluation of operational land imager sensor on board Landsat 8 and Landsat 9 for land use land cover mapping over a heterogeneous landscape", *Geocarto International*, Vol. 38(1), 2023.

[52]. P. Lemenkova, "Console-Based Mapping of Mongolia Using GMT Cartographic Scripting Toolset for Processing TerraClimate Data", *Geosciences*, Vol. 12(3), 140, 2022a.

[53]. P. Lemenkova, "GRASS GIS Scripts for Satellite Image Analysis by Raster Calculations Using Modules r.mapcalc, d.rgb, r.slope.aspect", *Tehnicki Vjesnik*, Vol. 29(6), 1956-1963, 2022b.

[54]. P. Lindh, and P. Lemenkova, "Evaluation of Different Binder Combinations of Cement, Slag and CKD for S/S Treatment of TBT Contaminated Sediments", *Acta Mechanica et Automatica,* Vol. 15(4), 236-248, 2021.

[55]. P. Lemenkova, "Random Forest Classifier Algorithm of Geographic Resources Analysis Support System Geographic Information System for Satellite Image Processing: Case Study of Bight of Sofala, Mozambique", *Coasts*, Vol. 4(1), 127-149, 2024c.

[56]. P. Lemenkova, "Automation of image processing through ML algorithms of GRASS GIS using embedded Scikit-Learn library of Python", *Examples and Counterexamples*, Vol. 7, 100180, 2025.

[57]. R. Li, L. Wang, G. Ou, W. Xu and Q. Dai, "Mapping Forest Type with Multi-Seasonal Landsat Data and Multiple Environmental Factors in Yunnan Province Based on Google Earth Engine," 2021 IEEE International Geoscience and Remote Sensing Symposium IGARSS, Brussels, Belgium, 2021, pp. 6468-6471, doi: 10.1109/IGARSS47720.2021.9554563.

[58]. J. Amorós-López, L. Gómez-Chova, L. Guanter, L. Alonso, J. Moreno and G. Camps-Valls, "Multitemporal fusion of Landsat and MERIS images," 2011 6th International Workshop on the Analysis of Multi-temporal Remote Sensing Images (Multi-Temp), Trento, Italy, 2011, pp. 81-84, doi: 10.1109/Multi-Temp.2011.6005053.

[59]. K. B, R. V, G. S and R. J, "Advanced Pansharpening Techniques for Satellite Image Fusion," *2024 International Conference on Power, Energy, Control and Transmission Systems (ICPECTS)*, Chennai, India, 2024, pp. 1-6, doi: 10.1109/ICPECTS62210.2024.10780411

[60]. Y. Gao, W. Zhang, J. Wang and C. Liu, "LULC classification of Landsat −7 ETM+ image from rugged terrain using TC, CA and SOFM neural network," 2007 IEEE International Geoscience and Remote Sensing Symposium, Barcelona, Spain, 2007, pp. 3490-3493, doi: 10.1109/IGARSS.2007.4423598

[61]. Y. S. Goh, W. Q. Chua, S. Yean and B. S. Lee, "Lessons from applying SRGAN on Sentinel-2 images for LULC classification," *2023 17th International Conference on Signal-Image Technology & Internet-Based Systems (SITIS)*, Bangkok, Thailand, 2023, pp. 107-114, doi: 10.1109/SITIS61268.2023.00025.

[62]. Y. Zheng, S. Liu, Z. Song, X. Tong and H. Xie, "Analyzing spatio-temporal characteristics of urban LULC and LST over Shanghai during 2009-2019," *2019 10th International Workshop on the Analysis of Multitemporal Remote Sensing Images (MultiTemp)*, Shanghai, China, 2019, pp. 1-4, doi: 10.1109/Multi-Temp.2019.8866897

[63]. A. Santangeli, O. Spiegel, P. Bridgeford, M. Girardello, "Synergistic effect of land-use and vegetation greenness on vulture nestling body condition in arid ecosystems", Scientific Reports 8, 13027 (2018). https://doi.org/10.1038/s41598-018-31344-2

[64]. W. Thuiller, G.F. Midgley, G.O. Hughes, B. Bomhard, G. Drew, M.C. Rutherford, F.I. Woodward, "Endemic species and ecosystem sensitivity to climate change in Namibia", *Global Change Biology*, 12, 2006, pp. 759-776. https://doi.org/10.1111/j.1365-2486.2006.01140.x

[65]. U. Dieckmann, "Thinking with relations in nature conservation? A case study of the Etosha National Park and Hai‖om", J R Anthropol Inst, 29, 2023, pp. 859-879. https://doi.org/10.1111/1467-9655.14008

[66]. A. Vushe, "Proposed Research, Science, Technology, and Innovation to Address Current and Future Challenges of Climate Change and Water Resource Management in Africa", 2021. In: Diop, S., Scheren, P., Niang, A. (eds) Climate Change and Water Resources in Africa. Springer, Cham. https://doi.org/10.1007/978-3-030-61225-2_21

[67]. R.G. Bryant, "Monitoring hydrological controls on dust emissions: preliminary observations from Etosha Pan, Namibia", *Geographical Journal*, 169, (2003, pp. 131-141. https://doi.org/10.1111/1475-4959.04977

[68]. S. van Asselen, P.H. Verburg, "Land cover change or land-use intensification: simulating land system change with a global-scale land change model", *Global Change Biology*, 19, 2013, pp. 3648-3667. https://doi.org/10.1111/gcb.12331